Proc. of the 6th WSEAS Int. Conf. on Signal Processing, Computational Geometry & Artificial Vision, Elounda, Greece, August 21-23, 2006 (pp160-169)

Bioacoustophotonic Depth-Selective Imaging of Turbid Media and Tissues: Instrumentation and Measurements

ANDREAS MANDELIS*
Center for Advanced Diffusion-Wave Technologies (CADIFT)
Dept. of Mechanical and Industrial Engineering
Univ. of Toronto
5 King's College Road, Toronto, Ontario, M5S 3G8
CANADA

Abstract: - In this paper I present recent trends in bioacoustophotonics of tissues. The presentation is centered on the development of Fourier-domain (frequency-swept) photothermoacoustic techniques to address issues associated with diffuse photon density waves during optical excitation of turbid media and soft tissues. These methods have concrete advantages over the conventional time-domain pulsed-laser counterparts. Theoretical and experimental results are presented in frequency-domain bioacoustophotonic detection and imaging. I describe the development of sensitive sub-surface imaging methodologies which hold the promise for sensitive diagnostics of cancerous lesions in e.g. a human breast. Results using tissue phantoms and *ex-vivo* specimens are discussed and the current level of sub-surface lesion sensitivity compared to state-of-the-art pulsed photoacoustic techniques is examined. In summary, advances in coupled frequency-domain diffuse-photon-density-wave and thermoelastic responses of turbid media constitute new trends in bioacoustophotonics which are quite promising for their signal quality and high dynamic range.

Key-Words: Biomedical photoacoustics, imaging, signal processing, depth-selective, turbid, tissue

1 Introduction

The field of bioacoustophotonics is the direct evolution of a rich arsenal of photothermal and photoacoustic techniques which have been under development for the past quarter century. The term "bioacoustophotonics" is itself an evolution of conventional photothermal and photoacoustic phenomena with the added complexity of optical propagation in turbid (scattering) tissue in which the heat- and/or sound-generating optical field is the result of diffuse photon density wave propagation in the medium[1]. From this perspective, the term indicates the coupled diffuse-photon-density wave sonar") and their applications to imaging of soft tissues. The mathematical coupling of diffuse-photon-density-wave and thermal-wave and thermal-wave phenomena in such media, followed by thermal-to-acoustical energy conversion and detection. Trends in improved diagnostic capabilities, coupled with significantly higher optical damage thresholds for tissue, point toward the use of frequency-domain (more precisely, Fourier-domain) techniques as the next-generation technologies to supplement or replace pulsed laser photothermal or photoacoustic detection with due attention to the physics of the photon propagation in the scattering medium. The field of laser bioacoustophotonics is introduced within the context of photothermoacoustic (PTA) swept-frequency-domain techniques ("PTA

propagation problems is an important issue toward the full development of the diagnostic opportunities of this area. The PTA approach to

non-invasive imaging of biomaterials takes advantage of high optical contrast of tissue chromophores and the ability of acoustic waves to travel long distances without significant distortion or attenuation. The general field of biomedical optoacoustics has so far been based entirely on pulsed laser excitation and time-of-flight measurements of acoustic transients to determine spatial position and optical properties of subsurface chromophores (blood vessels, tumors, tissue pigments and analyties 2-4]). The field has experienced very rapid development in recent years[5-7] due to promising results demonstrated in PTA experiments for depth profilometric measurements and imaging of turbid media at depths significantly larger than accessible by purely optical methodologies[2,8]. Although pulsed methods provide a number of advantages, there are certain difficulties for imaging applications and clinical implementation of the pulsed PTA technique. First, time-resolved measurements require wide-band (1 – 100 MHz) ultrasonic transducers – a very difficult or impossible technological challenge - and the signal-to-noise ratio (SNR) must be sufficiently high for wide detection bandwidths. Second, the inherently bipolar shape of acoustic transients and laser jitter noise compromise spatial resolution and render the precise measurement of subsurface chromophore position difficult. Third, the high peak power of laser pulses needed to deliver optical excitation to deep tissue layers may cause an adverse reaction in live human tissue. Last, but not least, time-domain methods cannot be used to perform operator-controlled depth-selective imaging. To overcome these difficulties of the pulsed PTA technique, a novel Fourier-domain photothermoacoustic (FD-PTA) depth-selective imaging methodology has emerged and will be described, featuring linear frequency modulated (LFM) optical excitation and coherent detection of the PTA response to determine the spatial position and optical parameters of sub-surface tissue chromophores. The main features of the FD-PTA technique are: a) the acoustic wave is generated by periodic modulation of a near-IR CW laser using LFM waveforms; b) depth information on sub-surface tissue structures is derived from the spectrum of the PTA signals; c) coherent signal processing is utilized to improve SNR; d) the time-domain PTA response is reconstructed from frequency scans using inverse Fourier transforms. The FD-PTA system can be used for both single-point depth profilometry and two-dimensional slice imaging of turbid media with optical absorption contrast at the wavelength of laser irradiation. Similar effects are expected with Fourier-domain PTA techniques. In communications systems, waveforms with linear frequency modulation have found extensive use in radar instrumentation as an alternative way to increase detection range while avoiding generation of high peak power pulses of radio waves [9]. Similar principles are also employed in tissue imaging by frequency domain optical coherence tomography (FD-OCT) [10]. High spatial resolution is achieved at the processing stage when a relatively long phase modulated signal is compressed into a narrow spike. Those techniques exhibit definite advantages over conventional pulsed methodologies: For example, frequency-swept FD-OCT has been demonstrated to provide higher acquisition speed and better signal-to-noise ratio ("sensitivity") advantages up to 30 dB [11,12] over time-domain OCT. The foregoing features are of critical importance in potential clinical applications of the FD-PTA technique, where optical pulse intensity and signal quality may be of real concern. Although such instrumentation and signal processing techniques are well established technologies in the field of remote detection and wireless communications, the FD-PTA approach to imaging of biological tissue is novel and original.

2. Frequency domain bioacoustophotonic imaging of soft tissues

2.1. Theoretical analysis of frequency-domain bioacoustophotonic signal generation

A mathematical model developed to study the laser-induced generation of acoustic waves in turbid media includes both the scattering and

absorption effects, and assumes the diffusion approximation of the radiative transfer equation[13] to describe the distribution of optical radiation in tissue. The geometry of optical excitation for a one-dimensional model representing a solid light-scattering layer positioned within a surrounding fluid is shown in Fig.1. The surrounding fluid represents an acoustic coupling medium between the probed solid and the transducer; it is assumed to have the physical properties of water, and occupies the spatial regions $-\infty < z \le -L$ and $0 \le z < \infty$. The fluid is characterized by density ρ_f and speed of sound c_f. The solid layer has thickness L, density ρ_s, speed of sound c_s, specific heat at constant pressure C_{ps}, optical absorption μ_a and scattering μ_s coefficients, bulk modulus K_s and isobaric volume expansion coefficient β_s. Analysis of acoustic wave generation in turbid media requires solution of a coupled boundary value problem involving equations for the radiative photon transport, the heat conduction and the acoustic pressure waves constrained by

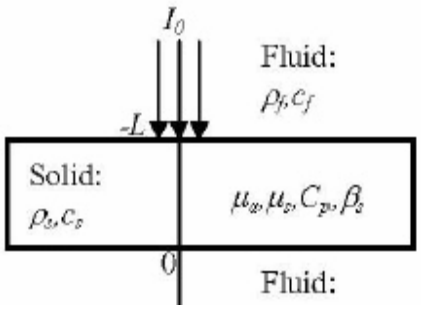

Fig. 1. One-dimensional geometry of photothermoacoustic effect in a light-scattering sample.

appropriate boundary conditions [14-17]. For a harmonic optical source, it is convenient to use frequency domain representations of the radiant fluence $\Psi(z,\omega)$, temperature $\theta(z,\omega)$ and acoustic pressure $P(z,\omega)$ that can be related to respective time-domain counterparts via a Fourier transform pair. A closed form solution can be derived for a one-dimensional geometry (Fig. 1) using the diffusion-wave transport equation:

$$\frac{\partial^2}{\partial z^2}\Psi_d(z,\omega) - \sigma_p^2 \Psi_d(z,\omega) = -\frac{S_0(z,\omega)}{D} \tag{1}$$

where Ψ_d is the diffuse scattered photon fluence, $\sigma_p^2 = (1 - i\omega\tau_a)/cD\tau_a$ is the diffuse photon wave number, $D = c/3(\mu_a+\mu_s')$ is the photon diffusion coefficient, $\mu_s' = \mu_s(1-g)$ is the reduced scattering coefficient, g is the scattering anisotropy factor, c is the speed of light in a sample, and $\tau_a = 1/c\mu_a$ is a characteristic time constant associated with the finite lifetime of photon diffusion from generation to absorption[16]. The source function $S_0(z,\omega) = \mu_s I_0 c(\mu_t+g\mu_a)/(\mu_t-g\mu_s)\exp[-\mu_t(z+L)]$, where I_0 is the laser fluence and $\mu_t = \mu_a+\mu_s$. Equation (1) must be complemented by boundary conditions for photon fluxes at both interfaces $z = -L$ and $z = 0$:

$$\Psi_d(-L,\omega) - A\frac{\partial}{\partial z}\Psi_d(-L,\omega) = -3\mu_s g A I_0$$

$$\Psi_d(0,\omega) + A\frac{\partial}{\partial z}\Psi_d(0,\omega) = 3\mu_s g A I_0 e^{-\mu_t(z+L)} \tag{2}$$

where $A = 2D(1 + r_{21})/c(1 - r_{21})$; r_{21} is the internal reflection coefficient, defined as the ratio of the upward-to-downward hemispherical diffuse photon fluxes. The total radiant fluence Ψ is composed of diffusive Ψ_d and coherent Ψ_c fields, $\Psi(z,\omega) = \Psi_d + \Psi_c$, and generates a photothermal source, the Fourier component of which is described by the thermal-wave equation:

$$\frac{\partial^2}{\partial z^2}\theta_s(z,\omega) - \sigma_s^2\theta_s(z,\omega) = -\frac{\mu_a \Psi(z,\omega)}{\kappa_s} \tag{3}$$

where $\theta_s(z,\omega)$ is the Fourier transform of the thermal source function, $\sigma_s^2 = (i\omega/\alpha_s)$ is the thermal wavenumber, and α_s and κ_s are, respectively, the thermal diffusivity and conductivity of the sample. Equation (3) must be accompanied by the continuity conditions for temperature and heat flux at the fluid-solid interfaces:

$$\theta_f(-L,\omega)=\theta_s(-L,\omega)$$
$$\kappa_s\frac{\partial}{\partial z}\theta_s(-L,\omega)=\kappa_f\frac{\partial}{\partial z}\theta_f(-L,\omega)$$
$$\theta_f(0,\omega)=\theta_s(0,\omega)$$
$$\kappa_s\frac{\partial}{\partial z}\theta_s(0,\omega)=\kappa_f\frac{\partial}{\partial z}\theta_f(0,\omega) \quad (4)$$

Finally, the spectrum $P(z,\omega)$ of laser-induced pressure waves in the surrounding fluid can be found from Helmholtz equations introducing the displacement potential $\phi_s(z,\omega)$ and the scalar potential $\zeta_f(z,\omega)$ of the fluid motion:

$$\frac{\partial^2}{\partial z^2}\phi_s(z,\omega)+k_s^2\phi_s(z,\omega)=\frac{K_s\beta_s}{\rho_s c_s^2}\theta_s(z,\omega)$$
$$\frac{\partial^2}{\partial z^2}\zeta_f(z,\omega)+k_f^2\zeta_f(z,\omega)=0 \quad (5)$$

where k_s and k_f are the acoustic wave numbers in the solid and fluid, respectively. Equations (5) are subject to boundary conditions for stress and displacement velocity:

$$\rho_s c_s^2\frac{\partial^2}{\partial z^2}\phi_s(0,\omega)-K_s\beta_s\theta_s(0,\omega)=i\omega\rho_f\zeta_f(0,\omega)$$
$$\rho_s c_s^2\frac{\partial^2}{\partial z^2}\phi_s(-L,\omega)-K_s\beta_s\theta_s(-L,\omega)=i\omega\rho_f\zeta_f(-L,\omega)$$
$$i\omega\frac{\partial}{\partial z}\phi_s(0,\omega)=\frac{\partial}{\partial z}\zeta_f(0,\omega)$$
$$i\omega\frac{\partial}{\partial z}\phi_s(-L,\omega)=\frac{\partial}{\partial z}\zeta_f(-L,\omega) \quad (6)$$

The solution of the coupled boundary-value problems (1)-(6) can be derived in closed form for one-dimensional geometry and was given in detail elsewhere [18]. The small-amplitude acoustic pressure change in the fluid is related to velocity potential as: $P(z,\omega) = -i\omega\rho_f\zeta_f(z,\omega)$ and can be written using the solution of Eqs.(5),(6) as:

$$P(z,\omega)=-i\omega\rho_f G e^{ik_f(z+L)} \quad (7)$$

where the complex valued constant G depends on the modulation frequency ω, on the sample optical and thermal properties, and on thickness L.

Theoretical simulations were performed for the simple case of a solid turbid layer immersed in water. Three input parameters, the optical absorption coefficient, optical scattering coefficient and thickness of the solid were changed independently for each simulation in order to analyze the time-domain PTA signal generation. Equation (7) was used to calculate the laser-induced acoustic field within a user-selected frequency range. The time-domain response was reconstructed from the computed spectrum using inverse Fourier transformation. Experimental verification was conducted using a heterodyne FD-PTA profilometric system described in earlier work [18] for the same range of modulation frequencies. These theoretical simulations demonstrate that the time-domain PTA response can be reconstructed from the frequency modulation scans and inverse Fourier transforms applied to the recorded PTA spectra. Although such measurements can be conducted using a standard lock-in amplifier, recording of frequency scans is very time consuming and would be impractical in real-life imaging applications. The instrumental implementation of the FD-PTA imaging system employs rapid frequency-swept (chirped) modulation of laser radiation, and a signal processing algorithm that relates the spectrum of the recorded PTA signals to the depth of sub-surface chromophores in tissue. The depth information in a LFM detection algorithm can be assessed by mixing the PTA signal with a replica of the modulation chirp. For example, let us assume the presence of a single subsurface chromophore, so that that the acoustic pressure signal thus generated is given by $P(t) = P_0 exp[i(2\pi f(t-\tau)t + \varphi_p)]$. Here P_0 is the amplitude, φ_p is the initial phase, $f(t) = f_0 + bt$ is the modulation chirp with frequency increase rate b, and $\tau = z_{ch}/c_a$ is the delay time of acoustic wave propagation from the depth z_{ch} with speed of sound c_a. Mixing $P(t)$ with a reference chirp $R(t) = exp[i2\pi f(t)t]$ and removing the sum frequency components in a low-pass filter (LPF), the combined signal becomes:

$$V(t)=\langle P(t)R(t)\rangle=\frac{P_0}{2}e^{-i(2\pi b\tau t-\varphi_p)} \quad (8)$$

The spectrum of the product contains the characteristic frequency $f_{ch} = b\tau = b(z_{ch}/c_a)$ proportional to the chromophore depth z_{ch}. In other words, the spectral content of $V(t)$ contains depth profilometric (or, more accurately, depth selective) information about the sub-surface chromophores. Since a weak PTA signal is normally contaminated by a significantly higher noise component, a lock-in detection technique can be employed to examine specific frequency ranges relevant to particular depths. Alternatively, cross-correlation detection with time-averaging can be used to increase the SNR of PTA measurements.

2.2. Experimental apparatus of the FD-PTA imaging system

Application of linear frequency modulated signals in radar (and sonar) instrumentation has found widespread use as an alternative way to increase detection range while avoiding generation of high peak power pulses of radio waves [19,20]. The optical analog of this technology was adopted in frequency-domain optical coherence tomography (OCT) for microscopic imaging of near-surface tissue structures [12,21]. Despite certain similarities in signal processing, those technologies differ from FD-PTA significantly by the fact that they detect echo responses rather than energy locally converted from optical flux to acoustic pressure wave via the thermoelastic effect. The implementation of the University of Toronto FD-PTA imaging system is shown in Fig. 2. It features a CW fiber laser (IPG Photonics) at the wavelength 1064 nm, an acousto-optic modulator (Neos Technologies) which is driven by signals from a function generator (Stanford Research Systems, DS345) and a focusing ultrasonic transducer (Panametrics) immersed in a water container for acoustic coupling. A test sample is positioned in water at the focal distance from the transducer. Optical radiation is modulated

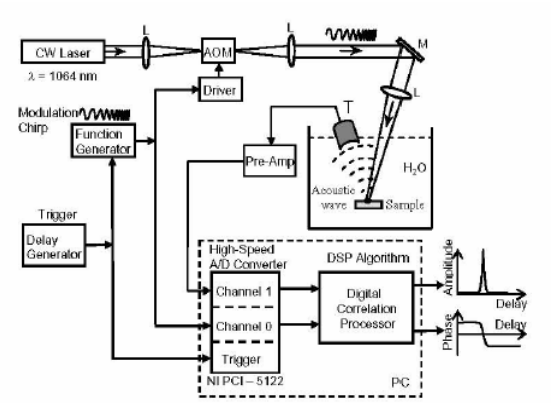

Fig. 2. Block diagram of the FD-PTA imaging system and signal acquisition schematics.

continuously by LFM waveforms in the range 1 MHz – 5 MHz at 1 ms repetition time. Modulation signal and data acquisition are triggered by a delay generator (Stanford Research Systems, DG535) and two signals (transducer voltage and reference chirp) are digitized simultaneously using a high-speed analog-to-digital converter (ADC) (National Instruments, PCI-5122) capable of maximum sampling rate of 10^8 samples/s. To process the acquired PTA signals, a software algorithm was designed and implemented, which employs digital correlation processing with respect to in-phase and quadrature modulation waveforms. This program simulates two virtual reference channels containing two chirps: a replica of the laser modulation and a chirp with 90-degree phase-shift introduced by a Hilbert transform. As shown in Fig. 3, the subsequent processing stages compute the cross-correlation of two reference waveforms with the signal received by an acoustic transducer. Low-pass filters recover in-phase V_I and quadrature V_Q components of the signal and, finally, amplitude and phase are computed as:

$$A(\tau) = (V_I^2+V_Q^2)^{1/2} \quad \text{and} \quad \phi(\tau) = \tan^{-1}(V_Q/V_I), \tag{9}$$

where τ is the delay time of reference chirps which can be varied within a pre-determined range. Since digital mixing and low-pass filtering effectively suppress all signals incoherent with a reference, the resulting amplitude is non-zero only for delays matching the arrival time of

frequency modulated acoustic waves from a test sample.

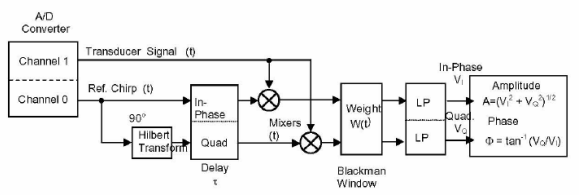

Fig. 3. Digital correlation processor with quadrature demodulation.

Plots in Fig. 4a and 4b show typical amplitude and unwrapped phase data for a noise-free chirp signal from a function generator delayed by 30 μs that simulates a PTA response.

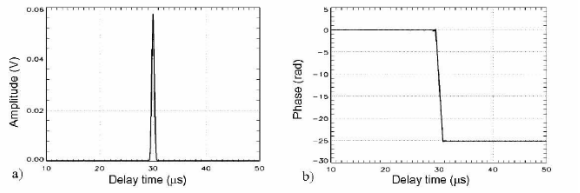

Fig. 4. Autocorrelation function amplitude (a) and phase (b) for a generator chirp signal delayed by 30 μs.

In the case of tissue which may include multiple discrete chromophores and background noise, the PTA signal is composed of a set of acoustic chirps with various amplitudes and delay times proportional to their depth. Therefore, demodulated amplitude data for a real tissue sample contain multiple peaks corresponding to different depths of tissue chromophores. Since chirp modulation is continuous, the PTA signal is averaged over multiple chirps and multiple scans to increase SNR. When the laser beam is scanned in the lateral direction, a 2-D slice PTA image can be reconstructed from consecutive depth (equivalent: time delay) scans. The depth resolution is determined by the width of the auto-correlation function which depends on the frequency-sweep rate *b*. The phase data may be used for depth selective profilometry and imaging as well, however the system noise contaminates in-phase and quadrature channels resulting in numerous discontinuities of the phase at ±π unrelated to the actual PTA signal. To take advantage of the phase channel, additional signal conditioning is required to ensure unambiguous phase measurements.

2.3. FD-PTA imaging of tissue phantoms and *ex-vivo* specimens

A series of test measurements with plastisol phantoms simulating tissue optical properties and *ex-vivo* tissue samples (chicken breast with embedded gel chromophores) were conducted to assess the depth-profilometric, depth-selective and imaging capabilities of the FD-PTA system. A focused acoustic transducer was used with the focal distance of 25.4 mm and peak sensitivity at 3.5 MHz. A high-frequency transducer provides superior spatial resolution because the width of the auto-correlation function is inversely proportional to the chirp bandwidth. In our experiments, width of the auto-correlation function was equal to 0.5 μs (FWHM), which translates approximately into 0.7 mm spatial resolution (assuming the speed of sound c_s = 1.48×10^5 *cm/s*). Fig. 5 shows an example of FD-PTA imaging of a planar absorbing inclusion (absorption coefficient μ_a= 4.2 cm^{-1}) positioned 6.3 mm deep inside a phantom with the reduced scattering coefficient μ_s' = 1.3 cm^{-1} and the ambient absorption μ_a = 0.5 cm^{-1}. The top surface of phantom (1) and the sub-surface inclusion interface (2) can be clearly visible as bright lines on the image.

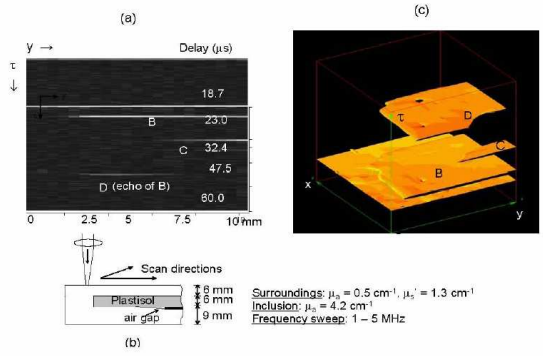

Fig. 5. (a) FD-PTA depth image of a planar light-absorbing inclusion (μ_a= 4.2 cm^{-1}) imbedded in a test plastisol phantom (μ_s'=1.3 cm^{-1}, μ_a=0.5

cm^{-1}) and scanning geometry. Label B indicates the extent of the plastisol phantom, C indicates the location of an airgap. All labels correspond to those shown in (c). The scale on the right refers to measured delay times τ in μs corresponding to the three-dimensional image (c). (b). Top arrows indicate phantom surface; bottom arrow points to artificial air gap under the inclusion. (c): Amplitude of two-dimensional scan across the surface resulting in a three-dimensional depth-selective image.

This image also reveals that acoustic waves reflected from mechanical discontinuities in the media appear as secondary sources in the PTA image. Arrow 3 indicates an artificial air gap under the inclusion which creates an acoustic impedance mismatch on the back surface. These studies have been extended to deeper inclusions and to three-dimensional imaging using x-y scans, as shown in Fig. 5(c). The depth selective capabilities of FD_PTA sub-surface imaging are clearly demonstrated in this figure. It should be noted that the presence of the airgap slice "C" below the layer "B" generates echo "D" and represents a high-impedance interface for the echo acoustic wave which manifests itself as a shadow of layer C projected onto layer "D".

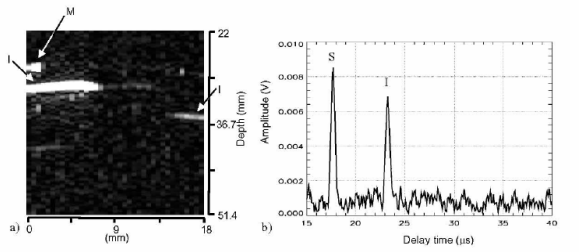

Fig. 6. FD-PTA imaging of chicken breast tissue: a) – chicken breast with two similar inclusions (absorption coefficient $\mu_a = 4$ cm^{-1}) positioned at different depths; b) – a single point depth scan for a deep (9±1 mm) inclusion in chicken breast. Arrow in the images: M – black ink marker on the tissue surface, I – imbedded inclusions, S- surface.

The next important step on the way to clinical applications of the FD-PTA technique is characterization of the system performance with real tissue specimens. A suitable model adequately representing optical and mechanical properties of human tissue is a chicken breast specimen with artificially embedded optical inhomogeneities simulating a cancerous tumor. An example of a two-dimensional FD-PTA slice image with two embedded gel inclusions with μ_a = 4 cm^{-1}, positioned 3 mm and 7 mm below the tissue surface is demonstrated in Fig. 6a. The position of inclusions is labeled as (I) and a black ink marker (M) indicates the tissue surface. The top surfaces of inclusions appear as thin bright lines on the image at different delay times. Their position can be clearly identified and measured in the FD-PTA image, even though the amplitude of signal from the deeper inclusion is significantly reduced. A relatively deep subsurface inclusion (9 ± 1 mm) in chicken breast is shown in Fig. 6b which represents a single spatial point measurement averaged over multiple scans to reduce the noise floor.

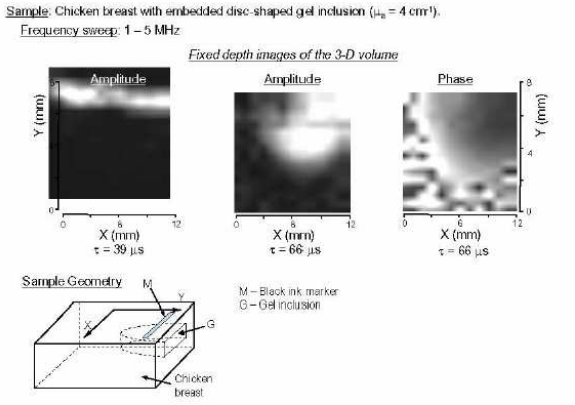

Fig. 7. Chicken breast with embedded disc-shaped gel inclusion.

A three-dimensional sub-surface image of a disk-shaped gel inclusion (chromophore) inside a chicken breast sample is shown in Fig. 7. In addition, a black line was drawn on the surface of the sample with a black ink marker as shown in the sample geometry. Fixing the delay time fixes the observation depth. The sequence of the three PTA images shown in the figure was obtained at delay time $\tau = 39$ μs (amplitude only) corresponding to the mean depth of the black ink line, and at 66 μs, corresponding to the mean depth of the gel inclusion. The complete time-

depth separation of the two features which are superposed in the same lateral coordinate range is very clear and is similar to the images shown in Fig. 5c. The amplitude image of the inclusion, however, carries a superposed image of the black line, because the PTA amplitude is a function of the incident laser intensity, which is compromised through optical absorption along the line of the black ink marker. On the other hand, the phase image of the inclusion does not show the black ink line: phase is independent of the intensity of the incident laser radiation as a ratio of the quadrature and in-phase lock-in signals and as such it construes a "true" photothermoacoustic image, independent of the optical properties of the surface. This characteristic of frequency-domain diffusion-wave fields has been reported in thermal-wave non-destructive imaging almost a quarter of a century ago [22], but has not found its bioacoustophotonic imaging analog until now. It is concluded that depth-selective PTA phase imaging can be a very important biomedical diagnostic tool, as it only depends on the local subsurface properties of the scanned sample (optical, thermal and acoustic), but not on optical beam intensity modification due to the presence of overlaying absorbing structures and/or laser power fluctuations. This is a feature worth investigating in greater detail in the future. The apparent structure in the $\tau = 66$ μs phase image of Fig. 7 is due to noise, as the absence of PTA signal outside the absorbing region at that depth renders the phase channel unstable. The noise can be easily filtered out using a simple algorithm that sets the phase equal to an appropriate value characteristic of the phase background.

Although directly comparable information is scarce, there is evidence that state-of-the-art biomedical pulsed photoacoustic systems with a single transducer can "see" sub-surface inhomogeneities in tissues at *ca.* 1 cm below the surface with a SNR of ~ 1.0 – 1.5 [23]. The sub-surface peak of Fig. 6b shows a far superior SNR and feature sharpness. It is encouraging that this is not an upper limit of the FD-PTA technique, because the SNR can be further improved with suitable signal averaging, wavelength optimization and transducer redesign, a promise for the detection of deep (>> 1 cm) sub-surface optical inhomogeneities.

Finally, preliminary tests with *in-vivo* tissue samples have been carried out to examine the

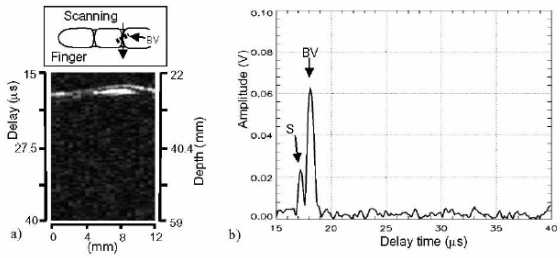

Fig. 8. A FD-PTA image of an index finger *in-vivo* (a) and a 1-D profile of amplitude recorded at the blood vessel position. Arrows on the plot: S – finger surface, BV – blood vessel.

sensitivity of the FD-PTA system to sub-surface chromophores typical to human tissue (epidermal melanin, blood vessels etc). A two-dimensional FD-PTA scan of an index finger of a healthy volunteer is shown in Fig. 8. The PTA signal from the finger surface is generated by light absorption in the epidermis while a discrete blood vessel appears as a localized increase in signal amplitude below. The separate contributions of the skin surface (S) and a blood vessel (BV) are shown in Fig. 9b which represents a single depth scan recorded at the blood vessel position identified in the 2-D image.

3. Conclusions

In conclusion, this paper has presented the concept of frequency-domain bioacoustophotonics, as distinct from pulsed laser detection for depth-selective soft tissue diagnostics. Bioacoustophotonics is the quantitative science and technology of the PTA detection of photon propagation in turbid biological media in which the thermal and acoustical energy conversion pathways serve to enhance the optical (spectroscopic) contrast of turbid tissue above the beyond the capabilities of purely optical methods: This is a coupled Boltzmann radiative tranfer, thermal and acoustic transport problem. Novel photothermoacoustic

imaging instrumentation systems have been described for noninvasive imaging of biological phantoms, *ex-vivo* and *in-vivo* tissues. The linear frequency modulated (chirped) optical excitation coupled with coherent signal processing provides dual channel (amplitude and phase) imaging capabilities compared to pulsed photoacoustic methods. Bioacoustophotonic depth-selective imaging can be used to perform sub-surface slice-by-slice image reconstruction from operator-determined, precisely-controlled depths. Frequency-domain PTA with a linear frequency-swept laser source and heterodyne detection provides depth localization of subsurface tissue chromophores with resolution < 1 mm and signal-to-noise ratio sufficient for noninvasive imaging in tissue 2 cm deep or better with a single transducer element. FD-PTA can be used to perform a single-point profilometric measurement as well as 2-D and 3-D imaging at precisely-controlled depths (depth selectivity). On the basis of similar comparisons with other frequency- and time-domain methods such as OCT [11,12], FD-PTA is expected to exhibit superior SNR at comparable depths than pulsed laser photoacoustics and may be applicable to biomedical imaging of blood rich tissue as in the case of sub-surface cancerous tumors.

ACKNOWLEDGMENTS

The support of the Natural Sciences and Engineering Research Council of Canada (NSERC) through a CHRP Grant is gratefully acknowledged. I wish to acknowledge my collaborators, Y. Fan, G. Spirou, S. Telenkov, A. Vitkin and W. Whelan for valuable contributions in many aspects of the development of the fields of frequency-domain bioacoustophotonics presented in this paper.

References:

[1] A. Mandelis, "Diffusion Waves and their Uses", *Physics Today*, **53**, Part I, 29-34, 2000.
[2] G. Andreev, A. A. Karabutov, S. V. Solomatin, E. V. Savateeva, V. Aleynikov, Y. Z. Zhulina, R. D. Fleming, and A. A. Oraevsky, *Biomedical Optoacoustics Proc. SPIE*, A. A. Oraevsky (ed), **3916**, 36-47, 2000.
[3] C. G. A. Hoelen, R. G. M. Kolkman, M. Letteboer, R. Berendsen and F. F. de Mul, "Photoacoustic tissue scanning (PATS)", *Optical Tomography and Spectroscopy of Tissue III Proc. SPIE*, **3597**, 336-343, 1999.
[4] P. C. Beard and T. N. Mills, "An optical detection system for biomedical photoacoustic imaging", *Biomedical Optoacoustics Proc. SPIE*, A. A. Oraevsky (ed), **3916**, 100-109, 2000.
[5] *Biomedical Optoacoustics Proc. SPIE*, A. A. Oraevsky (ed), **3916**, 2000.
[6] *Biomedical Optoacoustics II Proc. SPIE*, A. A. Oraevsky (ed), **4256**, 2001.
[7] A. J. Welch and M. C. van Gemert, Eds., *Tissue Optical Properties and Laser-Tissue Interactions*, AIP, New York, 1995.
[8] A.P. Gibson, J.C. Hebden and S.R. Arridge, "Recent advances in diffuse optical imaging", *Phys. Med. Biol*, **50**, R1-R39, 2005.
[9] M. I. Skolnik, *Radar Handbook*, McGraw-Hill, NY (1990).
[10] R. Huber, K. Taira, M. Wojtkowski, T. H. Ko, J. G. Fujimoto and K. Hsu, "High speed frequency swept light source for Fourier domain OCT at 20 kHz A-scan rate", Photonics West – Bios 2005, Coherence. Domain Optical Methods and Optical Coherence Tomography in Biomedicine, paper IX (BO114), 2005.
[11] J. F. de Boer, B. Cense, B. H. Park, M. C. Pierce, G. J. Tearney and B. E. Bouma, "Improved signal-to-noise ratio in spectral-domain compared with time-domain optical coherence tomography", Opt. Lett. **28**, 2067-2069, 2003.
[12] R. Leitgeb, C. K. Hitzenberger and A. F. Fercher, "Performance of fourier domain vs. time domain optical coherence tomography", Optics Express **11**, 889-894 (2003); M. A. Choma, M. V. Sarunic, C. Yang and J. A. Izatt, "Sensitivity advantages of swept source and Fourier domain optical coherence tomography", Optics Express **11**, 2183-2189 (2003).
[13] A. Ishimaru, *Wave Propagation and Scattering in Random Media Vol. 1*, Academic, New York, 1978.
[14] T. J. Farrell, M. S. Patterson and B. Wilson, "A diffusion theory model of spatially resolved,

steady-state diffuse reflectance for the noninvasive determination of tissue optical properties *in-vivo*", *Med. Phys.*, 19, 879-888, 1992.
[15] W. M. Star and J. P. A. Marijnissen, "New trends in photobiology (invited review) light dosimetry: status and prospects", *J. Photochem. Photobiol.*, **B1**, 149-167, 1987.
[16] A. Mandelis, *Diffusion-Wave Fields: Mathematical Methods and Green Functions*, Chap.10: 663 – 708, Springer-Verlag, New York, 2001.
[17] A. Karabutov and V. Gusev, *Laser Optoacoustics*, Chap. 2, AIP Press, New York, 1993.
[18] Y. Fan, A. Mandelis, G. Spirou and I.A. Vitkin, "Development of a laser photothermoacoustic frequency-swept system for subsurface imaging: Theory and experiment", *J. Acoust. Soc. Am.*, **116**, 3523-3533, 2004.
[19] M. I. Skolnik, *Radar Handbook*, Chap.10, McGraw-Hill, NY 1990.
[20] R.O. Nielsen, *"Sonar signal processing"*, Artech House, Boston, 1991.
[21] G. Hausler and M.W. Lindner, "Coherence radar and spectral radar- new tools for dermatological diagnosis", *J. Biomed. Optics*, **3**, 21-31, 1998.
[22] G. Busse, "Optoacoustic and photothermal material inspection techniques", Appl. Opt. **21**, 107-110, 1982.
[23] S. Manohar, A. Kharine, J.C.G. van Hespen, W. Steenbergen and T. G. van Leeuwen, "Photoacoustic mammography laboratory prototype: imaging of breast tissue phantoms", *J. Biomed. Opt.*, **9,** 1172-1181, 2004.